

1 **Comparison of modeled snow properties in Afghanistan, Pakistan, and Tajikistan**

2
3 Edward H. Bair¹, Karl Rittger², Jawairia A. Ahmad³, and Doug Chabot⁴

4
5 ¹Earth Research Institute, University of California, Santa Barbara, California, USA
6 6832 Ellison Hall, University of California, Santa Barbara, CA 93106-3060. correspondence
7 email: nbair@eri.ucsb.edu

8
9 ²Institute for Arctic and Alpine Research, University of Colorado, Boulder, Colorado, USA

10
11 ³Department of Civil & Environmental Engineering, University of Maryland, College Park, MD,
12 USA

13
14 ⁴independent researcher, Bozeman, MT, USA

15 ABSTRACT: Ice and snowmelt feed the Indus and Amu Darya rivers in western High Mountain
16 Asia, yet there are limited in situ measurements of these resources. Previous work in the region
17 has shown promise using snow water equivalent (SWE) reconstruction, which requires no in situ
18 measurements, but validation has been a problem. However, recently we were provided with daily
19 manual snow depth measurements from Afghanistan, Tajikistan, and Pakistan by the Aga Khan
20 Agency for Habitat (AKAH). To validate SWE reconstruction, at each station, accumulated
21 precipitation and SWE were derived from snow depth using the numerical snow cover model
22 SNOWPACK. High-resolution (500 m) reconstructed SWE estimates from the ParBal model were
23 then compared to the modeled SWE at the stations. The Alpine3D model was then used to create
24 spatial estimates at 25 km resolution to compare with estimates from other snow models.
25 Additionally, the coupled SNOWPACK and Alpine3D system has the advantage of simulating
26 snow profiles, which provide stability information. The median number of critical layers and
27 percentage of faceted layers across all of the pixels containing the AKAH stations was computed.
28 For SWE at the point scale, the reconstructed estimates showed a bias of -42 mm (-19%) at peak
29 SWE. For the coarser spatial SWE estimates, the various models showed a wide range, with
30 reconstruction being on the lower end. A heavily faceted snowpack was observed in both years,
31 but 2018, a dry year, according to most of the models, showed more critical layers that persisted
32 for a longer period.

33 1 INTRODUCTION

34 There are many parts of the world where little is known about the snowpack. This lack of
35 knowledge presents a challenge for water managers and for avalanche forecasters. Afghanistan is
36 particularly austere in this respect, as there have been no snow measurements available since the
37 early 1980s. This lack of information about the snowpack potentially creates a humanitarian crisis,
38 as snowmelt fed streams run dry in the fall without warning (USAID, 2008). Accurate historical
39 estimates of basin-wide snow water equivalent (SWE) are crucial for creating a baseline of
40 climatological conditions, which can then aid in predicting today’s SWE. For example, SWE
41 climatology is the most important predictor in machine learning statistical models for this region
42 (Bair et al., 2018a).

43 To improve our knowledge about the snowpack in these areas, we have developed an approach
44 that requires no in situ measurements. Using satellite-based estimates of the fractional snow-
45 covered area (fSCA) and downscaled forcings in an energy balance model, we build up the
46 snowpack in reverse, from melt out to its peak, using a technique called SWE reconstruction
47 (Martinec and Rango, 1981). This technique has been shown to accurately estimate SWE in
48 mountain ranges across the world, including: the Sierra Nevada USA (Rittger et al., 2016;Bair et
49 al., 2016); the Rocky Mountains USA (Jepsen et al., 2012;Molotch, 2009); and the Andes of South
50 America (Cornwell et al., 2016)—all areas with relatively abundant independent ground validation
51 measurements. For the so called Third Pole of High Mountain Asia, and especially the
52 northwestern parts of this region, e.g. Afghanistan, Tajikistan, and Pakistan, ground-based
53 validation is challenging.

54 2 AGA KHAN AGENCY FOR HABITAT (AKAH) STATIONS

55 In 2017, we received daily manual snow depth and other meteorological measurements from
56 nearly 100 stations (Figure 1) in an operational avalanche network (Chabot and Kaba, 2016). These
57 stations are funded by the Aga Khan Agency for Habitat (AKAH) and are the first snowpack
58 measurements available, at least that we are aware of, in Afghanistan in nearly 40 years. Hence,
59 we refer to the region as the AKAH study region and the weather stations as the AKAH stations.
60 The AKAH stations contain manual daily snow depth (also called height of snow), height of new
61 (24-hr) snow, daily high and low air temperature, instantaneous wind speed/direction, rainfall, and
62 some text fields on weather and avalanche conditions. For mountainous areas, precipitation is the
63 most uncertain term in the water balance (Milly and Dunne, 2002;Adam et al., 2006) because it
64 exhibits high spatial variability and is difficult to measure with traditional gauges. Measuring snow
65 on the ground has many advantages compared to using precipitation gauges, which suffer from
66 undercatch, especially in the windy and treeless areas (Lehning et al., 2002a;Kochendorfer et al.,
67 2017;Goodison et al., 1998) typical of this part of the world. Likewise, a strength of the SWE
68 reconstruction technique is that it does not depend on precipitation measurements to build the
69 snowpack.

70 Additionally, many of the AKAH stations are at high elevation, with 64 stations above 2500 m
71 and 17 stations above 3000 m. Unfortunately, most of these stations are located in deep valleys,
72 where the villages are, rather than on the mountains above and the daily resolution is too coarse to
73 use in a snow model without temporal interpolation. Additionally, many of the stations are near
74 glacierized areas which complicates spatially interpolated snow estimates, as some of the snow is
75 on top of ice. The area covered by glaciers in Figure 1 is 7.8%.

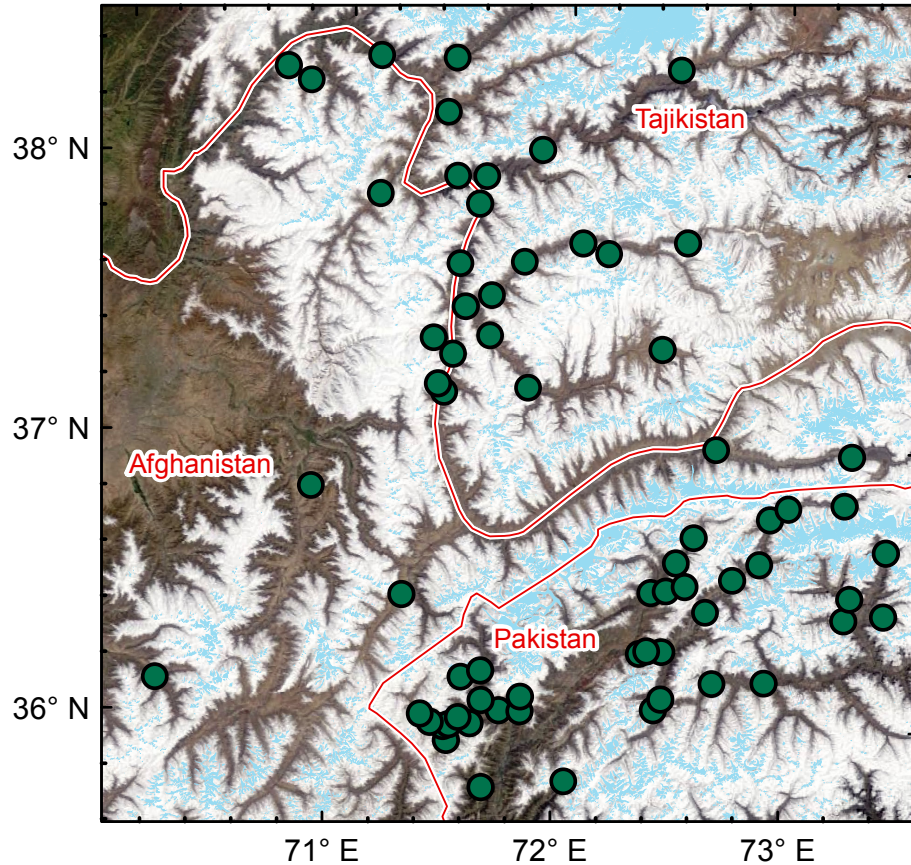


Figure 1 Study region with AKAH stations (green dots) overlaid on a MODIS true color image from 13 April 2018. Also shown are the country boundaries (red) and glacierized areas (light blue) from the Global Land Ice Measurement from Space dataset (Raup et al., 2007). All of the stations in Afghanistan and Tajikistan are in areas that eventually flow into the Amu Darya River. All of the stations in Pakistan are in areas that eventually flow into the Indus River.

76

77 Although there have been a large number of studies examining the glaciers of High Mountain Asia,
 78 there are fewer studies examining snowfall in High Mountain Asia, which is odd since
 79 hydrologically in this region, snow on land melt provides the vast majority of runoff compared to
 80 snow on ice and melting glacier ice (Armstrong et al., 2018). Many of these studies are focused on
 81 the region to the east of the AKAH study area shown in Figure 1. To our knowledge, there have
 82 been no studies on snowpack stratigraphy in the AKAH study area and we were unable to obtain
 83 any snow pit measurements from this area.

84 3 LITERATURE REVIEW

85 A few studies have specifically examined snowfall in larger regions that include some of the
 86 AKAH stations, mostly for stations in the southern basins that flow into the Indus River; that is all
 87 of the stations in Pakistan. The rest of the stations in Afghanistan and Tajikistan are in basins that
 88 flow into the Amu Darya River. The most comparable study (Shakoor and Ejaz, 2019) examines
 89 the Passu catchment in the Hunza River Basin, to the east of Figure 1. As in this study (Section
 90 5.1), Shakoor and Ejaz (2019) also use the SNOWPACK and Alpine3D models. Model parameters
 91 were calibrated using a single weather station, Urdukas at 3926 m elevation near the Baltoro glacier

92 (Ev-K2-CNR, 2014), with one year of precipitation measurements, using snow depth for
93 validation. The authors report overestimation of the measured snow depth at the calibration station,
94 even after questionable adjustments to the snow albedo and other model parameters. For example,
95 the snow and ice albedo is given as 0.20 to 0.30 (Table 3, Shakoor and Ejaz, 2019), which would
96 make it 0.10 to 0.20 lower than some of the lowest measured broadband albedo values for dirty
97 snow (Bair et al., 2019; Skiles and Painter, 2016). They attribute the overestimation to problems
98 with the precipitation measurements, common for high elevation stations. One problem with the
99 Urdukas station in particular is that the tipping bucket precipitation gauge is unheated, making it
100 unusable for measuring solid precipitation. Temperatures at this station were well below freezing
101 for the winter and most of the spring, which explains why no precipitation was recorded from
102 January until sometime in March during 2012, the calibration year.

103 Viste and Sorteberg (2015) study several gridded precipitation products throughout High Mountain
104 Asia, including the Indus River Basin. They report that while total precipitation was similar across
105 the products—including MERRA (Rienecker et al., 2011), APHRODITE (Yatagai et al., 2012),
106 TRMM (Huffman et al., 2007), and CRU (Harris et al., 2014)—the total snowfall varied by a factor
107 of 2 to 4. Smith and Bookhagen (2018) used 24 years (1987 to 2009) of satellite-based passive
108 microwave SWE estimates to examine trends throughout High Mountain Asia, including the Amu
109 Darya and Indus Basins. Their SWE estimates show most 25 km pixels in this region in the 50-
110 100 mm range for December through February, with a few over 100 mm in the Amu Darya (i.e.
111 all the AKAH stations in Afghanistan and Tajikistan) and none over 100 mm in the Indus (i.e. all
112 the AKAH stations in Pakistan), likely too low by an order of magnitude for some pixels given our
113 previous reconstructed SWE values and limited climate measurements in Afghanistan (Bair et al.,
114 2018a).

115 For the AKAH stations in Tajikistan, the most comprehensive snow measurements come from
116 Soviet snow surveys (mostly depth, but with some SWE and density measurements) that have been
117 digitized (Bedford and Tsarev, 2001). Most of these measurements begin in the late 1950s and end
118 around the fall of the Soviet Union, in either 1990 or 1992, making them useful for climatological
119 studies, but not for validation of modern satellite-based estimates.

120 The sole source of snow measurements in Afghanistan that were accessible to us was a table of
121 outdated WMO monthly climatological data from Kabul (el. 1791 m) and North Salang (el. 3366
122 m), showing the maximum monthly snow depth and the mean number of days with snow (Table 1
123 in Bair et al., 2018a). Again, these measurements are not useful to validate more modern snow
124 estimates.

125 There have been many other studies that have attempted to estimate basin-wide precipitation
126 (including snowfall) for larger areas that include the AKAH region, especially in the Indus. Several
127 climate studies of the Indus have focused on using lower elevation precipitation gauges, which are
128 then used to spatially interpolate basin-wide precipitation. Dahri et al. (2016) and Dahri et al.
129 (2018) have assembled perhaps the largest collection of climatological measurements covering the
130 AKAH region, mostly based on gauge measurements, as part of a study on the hydrometeorology
131 of the Indus Basin. Using undercatch corrections based on wind, often from reanalysis, they
132 increased precipitation estimates by 21% on average throughout the Indus Basin (Dahri et al.,
133 2018). For example, in the Gilgit sub-basin, they find an unadjusted precipitation estimate of 582
134 mm/year, adjusted to 787 mm/year, a 35% increase. Although some of the measurements are taken
135 from publicly available sources, as with most publications for this region, the comprehensive data
136 used are not publicly accessible.

137 A similar but less sophisticated approach was used by Lutz et al. (2014), who used a constant
138 increase of 17% across the APHRODITE precipitation dataset which covers all of High Mountain
139 Asia. Immerzeel et al. (2015) used glacier mass balance estimates with streamflow measurements
140 as validation to show that high-altitude precipitation in the upper Indus Basin is 2 to 10 × what is
141 shown using gridded precipitation products like APHRODITE. Bookhagen and Burbank (2010)
142 estimate that snowmelt contributes 66% of annual discharge to the Indus, and averages 424 mm
143 across the basin.

144 In summary, quite a few studies have produced varying precipitation and snowfall estimates for
145 the AKAH region, with no recent in situ snow measurements from Afghanistan or Tajikistan.

146 4 PREVIOUS WORK WITH AKAH SNOW MEASUREMENTS

147 Our previous work (Bair et al., 2018a) used a simple density model (Sturm et al., 2010) based on
148 snow climatology (Sturm et al., 1995) and day of year to model SWE from the manual snow depth
149 measurements. The density model itself has -12 to 26% bias in predicting SWE. When taking into
150 account geolocational uncertainty of the reconstructed SWE estimates and uncertainty in the
151 density model, errors are on the order of 11-13% Mean Absolute Error (MAE) and -2 to 4% bias,
152 depending on the date. However, we only examined one year of the AKAH station data (2017)
153 and the high uncertainty in the density model itself begs a more sophisticated approach.

154 From recent work (Bair et al., 2018b), we have shown that the SNOWPACK (Lehning et al.,
155 2002b;Lehning et al., 2002a;Bartelt and Lehning, 2002) model is capable of accurate SWE
156 prediction when supplied only with snow depth for precipitation, as well as the other requisite
157 forcings (i.e. radiation, snow albedo, temperatures, and wind speed). Over a 5-year period using
158 hourly in situ measured energy balance forcings and a snow pillow for validation at a high
159 elevation site in the western US, the numerical snow cover model SNOWPACK modeled SWE
160 showed a bias of -17 mm or 1% (Bair et al., 2018b). Likewise, the success of the Airborne Snow
161 Observatory (Painter et al., 2016) has demonstrated that given accurate snow depth measurements,
162 SWE can be well modeled.

163 5 METHODS

164 Our modeling approach consisted of: a) downscaling forcings in ParBal and reconstructing SWE;
165 b) combining the downscaled forcings for each AKAH station with temporally interpolated manual
166 snow measurements; c) running SNOWPACK for each of the AKAH stations with the downscaled
167 and interpolated measurements from a) and b); and d) running Alpine3D using the output from
168 SNOWPACK, notably the hourly precipitation. In addition to predicting SWE, the
169 SNOWPACK/Alpine3D coupled model also predicts stratigraphic parameters useful for avalanche
170 forecasting, thereby giving us an idea of the layering and stability in this region. For comparison,
171 we also ran the NOAH-MP land surface model over the region with widely-used forcings. We also
172 compared spatial estimates of SWE from GLDAS-2. Methods are summarized in Table 1 and
173 explained below, with more detail provided in Appendix A.

174 5.1 SNOWPACK and Alpine3D

175 SNOWPACK and Alpine3D are freely available (<https://models.slf.ch>) point and spatially
176 distributed snow models, courtesy of the Swiss Snow and Avalanche Research Institute SLF.

177 SNOWPACK is the older of the two and uses finite elements to model all of the layers in a
 178 snowpack at a point.

| Model | Point comparison? | Spatial comparison? | Version | Forcings | Output |
|----------|-------------------|---------------------|-------------|---|---|
| ParBal | √ | √ | 1.0 | CERES 4a (radiation); GLDAS-2 (meteorological); MODSCAG/MODDRFS (snow surface properties) | Daily reconstructed SWE at 500 m; hourly downscaled forcings at 500 m, both for entire AKAH study area |
| SNOWPACK | √ | | 3.5 | AKAH station snow measurements; downscaled forcings from ParBal | Hourly SWE, precipitation, and other forcings for each AKAH station |
| Alpine3D | | √ | 3.1 | AKAH station output from SNOWPACK | Daily SWE at 25 km for entire AKAH study area |
| NOAH MP | | √ | 3.6 | MERRA-2 | Daily SWE at 25 km for entire AKAH study area |
| GLDAS | | √ | NOAH 2.1 | various | Daily SWE at 25 km for entire AKAH study area |

179 *Table 1 Summary of models used. See Section 5 and Appendix A for an explanation of acronyms and further*
 180 *details.*

181 SNOWPACK has shown promising results in both operational (e.g. Lehning et al.,
 182 1999;Nishimura et al., 2005) and research applications (e.g. Bellaire et al., 2011;Hirashima et al.,
 183 2010). Previous results with SNOWPACK (Bair et al., 2018b) show high model sensitivity to
 184 precipitation, but only a 1% error in modeled SWE when using snow depth only (not total
 185 precipitation) as a forcing. Thus, given reliable snow depth measurements at each AKAH station
 186 (see Section 5.5), modeled SWE during the accumulation season is treated as having negligible
 187 uncertainty. During the ablation season (after peak SWE), uncertainty is higher. Unlike during
 188 snow accumulation events, SNOWPACK does not force its modeled snow ablation to match the
 189 measured snow depth decreases. Uncertainty in SWE during the ablation season is then largely
 190 dependent on radiative forcings (Marks and Dozier, 1992) and the broadband snow albedo (Bair
 191 et al., 2019). Here, 5% uncertainty is used, based on the MAE from SWE reconstructions using
 192 the same remotely-sensed forcings at a continental sub-alpine site (Bair et al., 2019). In the same
 193 study, a small (3%) bias in SWE was also found, but this is likely due to shortcomings with the
 194 reconstruction method and not applicable to SWE modeled with SNOWPACK. Thus, the small

195 bias was ignored. We acknowledge that these uncertainty estimates are themselves uncertain, e.g.
196 the reanalysis forcings could be especially poor for this region compared to those available in the
197 western US.

198 Alpine3D (Lehning et al., 2006) is essentially a spatially-distributed version of SNOWPACK with
199 a number of additional modules including: terrain-based radiation modeling, blowing snow, and
200 hydrologic modeling. Integral to Alpine3D is SNOWPACK, which is run for each pixel, as well
201 as the MeteIO library (Bavay and Egger, 2014), which provides a large number of temporal and
202 spatial interpolation functions that can be used on forcings for Alpine3D and SNOWPACK.

203 *5.2 The Parallel Energy Balance Model*

204 The Parallel Energy Balance Model (ParBal) was created at UC-Santa Barbara and designed for
205 reconstruction of SWE. It is also publicly available
206 (<https://github.com/edwardbair/ParBal/releases/tag/v1.0>). Currently, ParBal is designed to use:
207 downscaled temperature, pressure, and humidity from version 2 of the Global or National Land
208 Data Assimilation System (GLDAS-2/NLDAS-2, Xia et al., 2012; Rodell et al., 2004); shortwave
209 and longwave radiation from edition 4a of the Clouds and the Earth's Radiant Energy System
210 (CERES, Rutan et al., 2015) SYN product; and time-spaced smoothed (Dozier et al., 2008; Rittger
211 et al., in press) snow surface properties from MODIS Snow Covered Area and Grain Size
212 (MODSCAG, Painter et al., 2009) and MODIS Dust and Radiative Forcing in Snow (MODDRFS,
213 Painter et al., 2012). ParBal is run hourly at 500 m spatial resolution and forcings are adjusted for
214 terrain and elevation. The main output is the residual energy balance term, which is assumed to go
215 into melt when positive during the ablation phase after cold content is overcome (Jepsen et al.,
216 2012). This residual melt term is then summed in reverse during periods of contiguous snow cover
217 and multiplied by the fSCA to spread the snow spatially. The errors in SWE from ParBal are
218 mostly from fSCA and the radiative forcings. Errors and details on ParBal are covered extensively
219 in Bair et al. (2016) and Rittger et al. (2016). In the supplement for Bair et al. (2018a), the errors
220 arising from using GLDAS-2 and CERES 4a (available worldwide but at coarser spatial resolution)
221 vs. NLDAS-2 are specifically evaluated. Using three years of basin-wide SWE estimated by the
222 Airborne Snow Observatory in the upper Tuolumne Basin, California USA, the MAE for ParBal
223 was 25 mm or 26% (Bair et al., 2018a).

224 *5.3 Global Data Assimilation System 2 (GLDAS-2)*

225 For comparison, we also include the SWE estimates from GLDAS-2 (Noah). SWE from GLDAS-
226 2 has been shown to be comparable to estimates from other reanalysis datasets, but negatively
227 biased by about 60% in comparison to higher spatial datasets with assimilation from snow station
228 measurements (Broxton et al., 2016).

229 *5.4 NOAH Multi-Parameterization (MP)*

230 The NOAH-MP v3.6 (Niu et al., 2011; Ek et al., 2003) land surface model, forced using MERRA-
231 2 (Gelaro et al., 2017), was used to simulate the hydrologic cycle over the study area and provide
232 SWE estimates for comparison with ParBal and the Alpine3D output. NOAH-MP was selected
233 due to its detailed representation of the snowpack relative to other land surface models. The model
234 subdivides the snowpack into up to three layers with associated liquid water storage and
235 melt/refreeze capability (Yang and Niu, 2003; Niu and Yang, 2004). It incorporates the exchange

236 of heat and moisture through the snowpack between the land surface and the atmosphere. In a
237 model intercomparison study using a 2 km spatial resolution regional climate model for forcings,
238 Chen et al. (2014) show that NOAA-MP modeled peak SWE at SNOTEL sites in Colorado, USA
239 with a -7% bias.

240 5.5 Use of AKAH station measurements

241 We modeled daily SWE at the AKAH stations during the 2017 and 2018 water years (WY)
242 primarily using the manually measured height of snow (HS), also called snow depth, combined
243 with our downscaled energy balance parameters (for downscaling methodology see Rittger et al.,
244 2016;Bair et al., 2016;Bair et al., 2018a). To our knowledge, no quality control was performed on
245 the AKAH station measurements before we received them. We choose the manual HS and new
246 (24-hr) snow (HN) as the only variables to use from the AKAH stations. The HS appeared to be
247 the most reliably measured, as that only requires reading a value from a master snow depth stake.
248 Apart from spurious drops or missing values (see below), the HS measurement appeared consistent
249 and believable at most of the stations, implying an accurate snow depth record. The HN was used
250 to correct a data entry problem in 2017 that we discuss below. The reliability of the other
251 measurements (instantaneous wind speed/direction, maximum/minimum temperature, and
252 rainfall) was questionable. For example, we were not provided with sensor or measurement
253 metadata, e.g. sensor make/model, measurement height, and whether or not the temperature sensor
254 was shielded from shortwave radiation. These other measurements taken daily were also of limited
255 value for interpolation to hourly values (see item 3 below). Thus, these other measurements were
256 not used.

257 The AKAH dataset had a number of shortcomings that we list here along with how we addressed
258 them.

- 259 1) Some of the stations recorded no snow at all, especially in the dry 2018 year, or had obvious
260 problems, such as weeks of missing measurements, so they were excluded. For 2017, 52 (54%)
261 of stations were used. For 2018, 41 (46%) stations were used.
- 262 2) There were spurious drops in the HS measurements. The drops were clearly cases of missing
263 values being filled with zeros. These measurements were manually flagged and converted to
264 null values for interpolation, see below.
- 265 3) The daily measurements had to be interpolated to hourly values. For the most part we used
266 linear interpolation, although this is not ideal during snow accumulation since it's almost never
267 the case that snowfall is uniform over a 24-hr period. This is a problem that affects the accuracy
268 of snow settlement estimated by SNOWPACK. There were two cases where other interpolation
269 methods were used. If there were several days of missing values, we used a nearest neighbor
270 interpolation to fill in the missing daily values, followed by a linear interpolation from daily to
271 hourly measurements such that we assumed all the new snow fell in a 24-hr period. The other
272 case was for days where the linear interpolation would yield a value below the minimum
273 threshold hard coded into SNOWPACK (0.5cm/hr) for the first accumulating snowfall on bare
274 ground. In this case, a previous neighbor interpolation was used in such a way that the entire
275 snowfall occurred in the last hr prior to the next day's measurement.
- 276 4) We found the AKAH stations suitable for snow on the ground measurements, but not for
277 rainfall or total (solid+liquid) precipitation. This was only an issue for the Alpine3D snow
278 modeling, as snow measurements were being extrapolated to higher elevations than the AKAH

279 stations (Section 6.2), thus at these higher elevations, snow accumulated earlier and melted
280 later than at the lower AKAH stations.

281 Given the near total lack of canopy cover in the region, we suspected substantial undercatch from
282 rain gauges. Using the wind speed, an undercatch correction would have been possible given more
283 information on the gauges (e.g. orifice opening diameter and whether or not a shield was present),
284 however this instrument metadata was not available to us. Likewise, we did not know if the gauges
285 were heated or not.

286 Further, the time period for recording measurements from the stations was not consistent. In WY
287 2017, measurements began being reported on 10 November 2016 and were reported until 24
288 November 2017. However, in WY 2018, measurements weren't reported until 1 December 2017
289 and no station measurements were reported past 1 April 2017. The reporting period likely covered
290 all the snowfall events, but not all the precipitation events.

291 To address the rainfall measurement and reporting issues, we used GLDAS NOAH v2.1 (Rodell
292 et al., 2004) rainfall + snowfall from the nearest grid cell (1/4° spatial / 3 hr temporal resolution)
293 to fill in precipitation prior to the first measurements in each water year, and after 4-1 for both
294 water years. We did not account for rain from 10 November 2016 to 1 April 2017 and from 1
295 December 2017 to 1 April 2018; instead we relied on the modeled precipitation from SNOWPACK
296 using snow depth. The AKAH station observations show that rain during this time period was rare.

297 5) A database problem prevented snow heights > 100 cm from being entered into the database for
298 a few days in 2017. This problem became apparent during February 2017, when the Nuristan
299 avalanches took place (United Nations, 2017), as that is the first time that most stations
300 recorded values > 100 cm. Values were shown as 100 cm on multiple days followed by values
301 > 100 cm. To address this issue, we flagged all the values equal to 100 cm prior to peak snow
302 depth in 2017, then marked those as null values. We then filled those null values using the
303 cumulative sum of new snow during that time.

304 *5.6 Analysis of modeled snow profiles*

305 For holistic measures of the snow profiles modeled in Alpine3D, we used two metrics from
306 Bellaire et al. (2018): 1) fraction of facets and 2) number of critical layers. Fraction of facets is the
307 height of all the layers containing faceted crystals, i.e. International Classification for Seasonal
308 Snow on the Ground primary codes FC, DH, and SH (Fierz et al., 2009), divided by the height of
309 the snowpack. The number of critical layers was computed using a threshold sum approach
310 (Schweizer and Jamieson, 2007) with modifications for simulated profiles (Monti et al., 2014
311 Table 1). In each profile, 6 different variables (grain size, difference in grain size, hardness,
312 difference in hardness, grain type, and depth) in the top meter of the snowpack (from the surface)
313 were checked against threshold values. Layers exceeding 5 or more thresholds were classified as
314 critical.

315 The fraction of facets metric does not have a validation study, but faceted layers are a weak crystal
316 form and are responsible for 43% (Bair et al., 2012) to 67% (Schweizer and Jamieson, 2001) of
317 investigated avalanches. Layers classified as critical using the threshold sum approach above
318 corresponded to failure layers about half of the time to failure layers found with Compression Tests
319 (Monti et al., 2014), an in situ snowpack stability test (van Herwijnen and Jamieson,
320 2007;Jamieson, 1999).

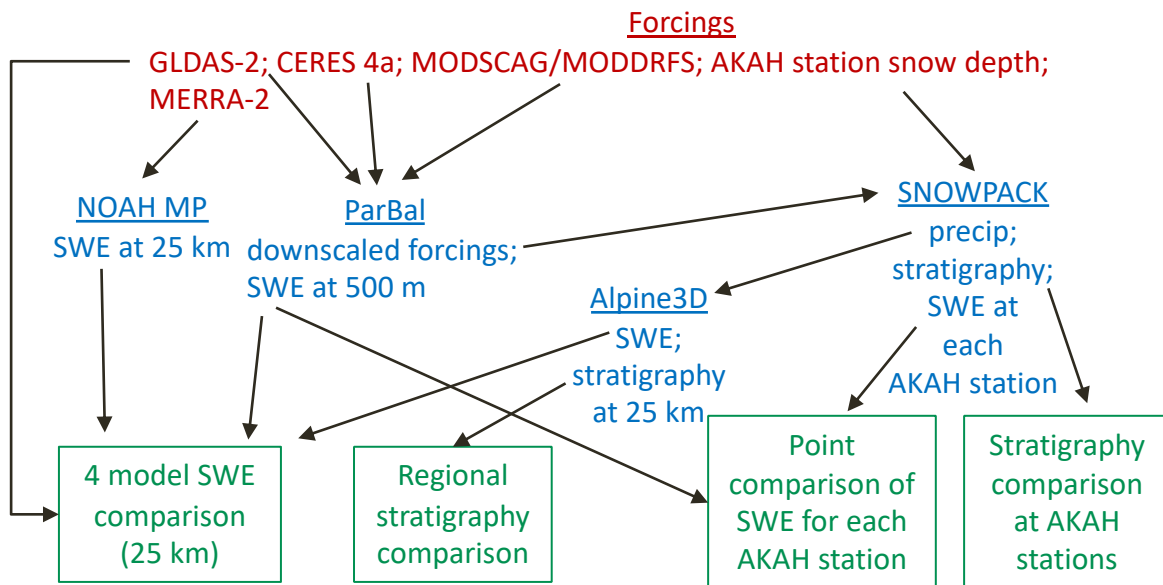
321 5.7 Spatial scale for comparisons

322 Because ParBal is the only model run at 500 m spatial resolution and all the other models were run
 323 at ~25 km, it is the only model appropriate for point comparisons, although point to area problems
 324 are still an issue. To address the geolocational uncertainty for the gridded MODIS products, which
 325 can be up to one ~500 m pixel (Tan et al., 2006; Xiaoxiong et al., 2005) and spatial variability of
 326 the snow, we used a 9-pixel neighborhood centered on each AKAH station and chose the best fit
 327 to the SNOWPACK modeled SWE. This approach has been used in previous work (Bair et al.,
 328 2018a; Rittger et al., 2016). We also include the high and low SWE values in that surrounding 9-
 329 pixel neighborhood to bound the uncertainty.

330 For all of the other model comparisons, we resampled all of the model output to a UTM (Zone
 331 43S) grid with 25 km pixels, close to the native resolution of the NOAH-MP and GLDAS2 grid
 332 used (0.25°). This yielded a study area of 105,625 km² (13 x 13 pixels, each 25 km² in area). The
 333 ParBal output had to be significantly upscaled from 500 m to 25 km using Gaussian Pyramid
 334 reduction (Burt and Adelson, 1983) in steps with bilinear interpolation for the final step.

335 6 RESULTS AND DISCUSSION

336 The relationships between the components are summarized in Figure 2. The results discussed
 337 below are comparisons of: 1) SWE and 2) snow stratigraphy across a) all of the AKAH stations
 338 (points) and b) the entire study region.



339 Figure 2 Summary of relationships between the various components. Forcings are shown in red, models and selected outputs are shown in blue, and the comparisons discussed below are shown in green. The black arrows show the direction of inputs.

340 6.1 Point comparisons between SNOWPACK and reconstructed SWE

341 A first step for any SWE reconstruction comparison is to determine when the ablation season starts.
 342 This varies for different years and at different sites (e.g. Margulis et al., 2016). Using the

343 SNOWPACK modeled SWE, we can examine the peak SWE dates for both years for all of the
 344 AKAH stations (Figure 3ab). Peak SWE dates vary across the stations and years, but the median
 345 values between years are a week apart, 19 February 2017 and 26 February 2018. Thus, we use
 346 those dates for our comparisons.

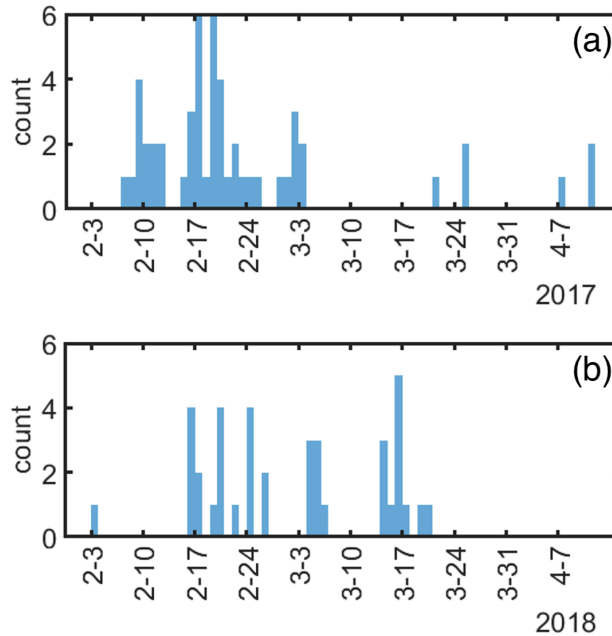


Figure 3 Peak SWE dates, modeled by SNOWPACK for 2017 (a) and 2018 (b) for each of the AKAH stations. The median peak SWE dates are 19 February 2017 and 26 February 2018. $N=52$ and 41 AKAH stations used for 2017 and 2018.

347

348 To create a holistic comparison for all the stations across the ablation period, mean SWE values
 349 were computed and plotted for each day during the ablation season (Figure 4). For the
 350 reconstructed SWE on 19 February 2017, the bias is -77 mm (-28%). For the reconstructed SWE
 351 on 26 February 2018, the bias is -6 mm (-9%). Thus, together these biases average to -42 mm ($-$
 352 19%). The high/low values in the 9-pixel neighborhood show the wide spatial variation in SWE
 353 estimates, and are to be expected in these deep valley sites (Section 6.2). The increases in
 354 reconstructed SWE during the ablation season are caused due to differences in how melt is summed
 355 for any given pixel. In ParBal, melt is only summed during periods of contiguous snow cover. This
 356 means that if a pixel containing an AKAH station has no snow on it at some point during the
 357 ablation season, but then snow is detected, it causes an increase in the mean SWE. This is called
 358 an ephemeral snow event, i.e. snow that disappears and reappears. For a more in depth examination
 359 of the error at individual stations, a box plot is shown for the median peak SWE dates for both
 360 years (Figure 5). The median bias of the reconstructed SWE is -11 mm (-14%).

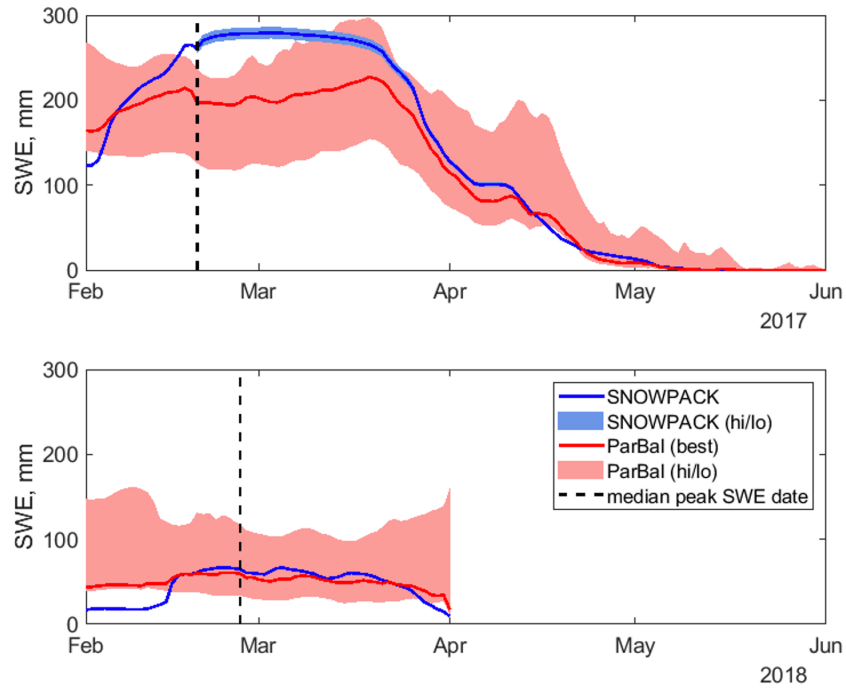


Figure 4 Mean SWE for 2017 (a) and 2018 (b) modeled at all of the AKAH stations using SNOWPACK (blue lines) compared to reconstructed SWE from ParBal using a best of 9-pixel approach (red lines). Also plotted is the median peak SWE date. The hi/lo bounds (filled areas) represent uncertainty. For ParBal, uncertainty is expressed as the range of values in the 9 pixel neighborhood. For SNOWPACK, uncertainty is 5% of the modeled SWE during the ablation season. See Sections 5.1 and 5.2 for details. The modeled SWE values end abruptly on 1 April 2018 because the AKAH stations stopped reporting due to drought conditions. The number of stations used is the same as in Figure 3.

361

362

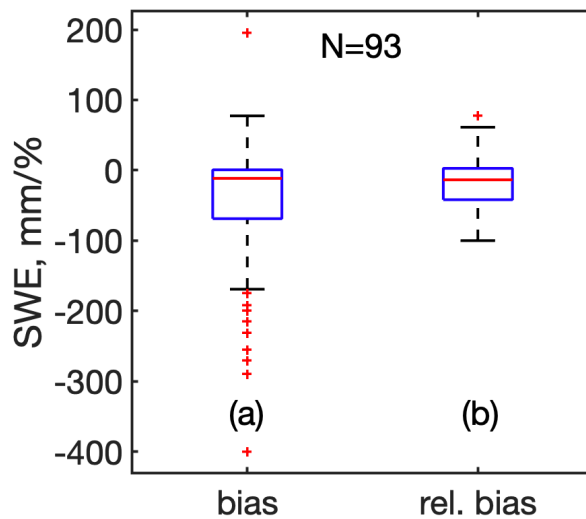


Figure 5 Bias (a) and relative bias (b) for ParBal reconstructed SWE vs Alpine 3D modeled SWE at AKAH stations on the median peak SWE date for both years, where bias here is ParBal SWE – Alpine 3D SWE.

363

364 6.2 Four model spatial comparisons

365 The AKAH stations are lower than the average elevation for the region. The average elevation of
 366 the AKAH stations is 2619 m (1735 to 3410 m). But when the 500 m DEM is upscaled to 25 km,
 367 the average elevation of the pixels containing the AKAH station is 3858 m with a range of 2517
 368 to 4764 m. This has two important implications: 1) much of the higher elevation snowfall is being
 369 extrapolated and 2) the higher elevation causes the peak SWE date to move forward in time. The
 370 median peak SWE dates for the (N=169) 25 km pixels encompassing the study area are 5 May
 371 2017 and 3 May 2017. Thus, we use the median of the two to compare our reconstructed SWE
 372 values (Figure 6ab, Figure 7a-d, and supplementary video).

373 Striking is the range between models. NOAH-MP has the highest peaks (562 mm in 2017 and 331
 374 mm in 2018), but is among the first to melt out. The reconstructed SWE from ParBal only shows
 375 minor variation between the 2017 peak (240 mm) and the 2018 peak (206 mm). ParBal and
 376 GLDAS-2 melt snow out latest in both years. This is especially true for ParBal in 2017, where the
 377 supplementary video shows that ParBal has snow cover over more pixels that persists for longer
 378 into the melt season, but is lower in SWE than the other models. The Alpine 3D model shows the
 379 second highest peak SWE in 2017 (469 mm), but the lowest peak (165 mm) in 2018. The
 380 comparatively higher values from NOAH-MP could result from relatively high precipitation
 381 estimates from its MERRA2 precipitation forcings. Similarly, Viste and Sorteberg (2015) report
 382 that MERRA (version 1) showed higher snowfall in the Indus Basin than any other reanalysis or
 383 observation-based forcings dataset.

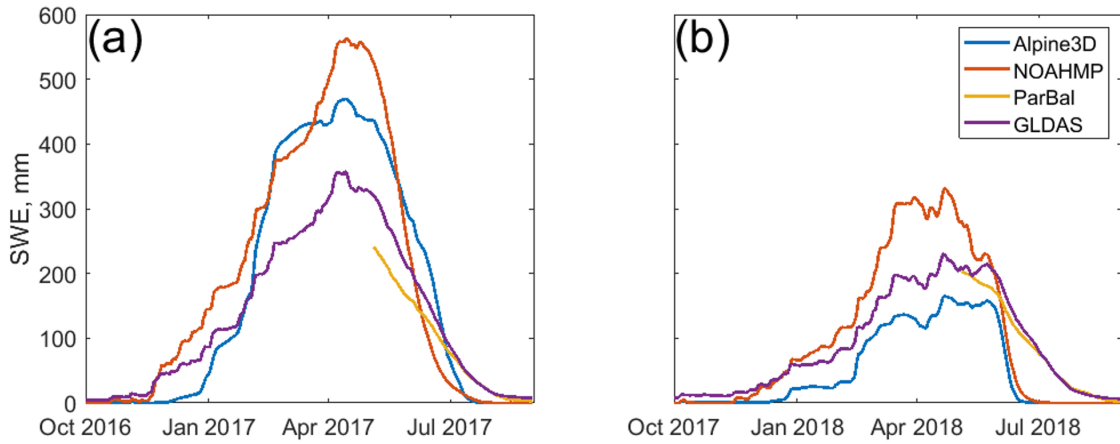


Figure 6 Time series of mean SWE for four snow models across the study area (13x13x25 km pixels) shown in Figure 1 for 2017 (a) and 2018 (b). The reconstructed SWE from ParBal (yellow) goes back to 4 May, the median peak SWE date for both years, since reconstruction is only valid during the ablation season.

384

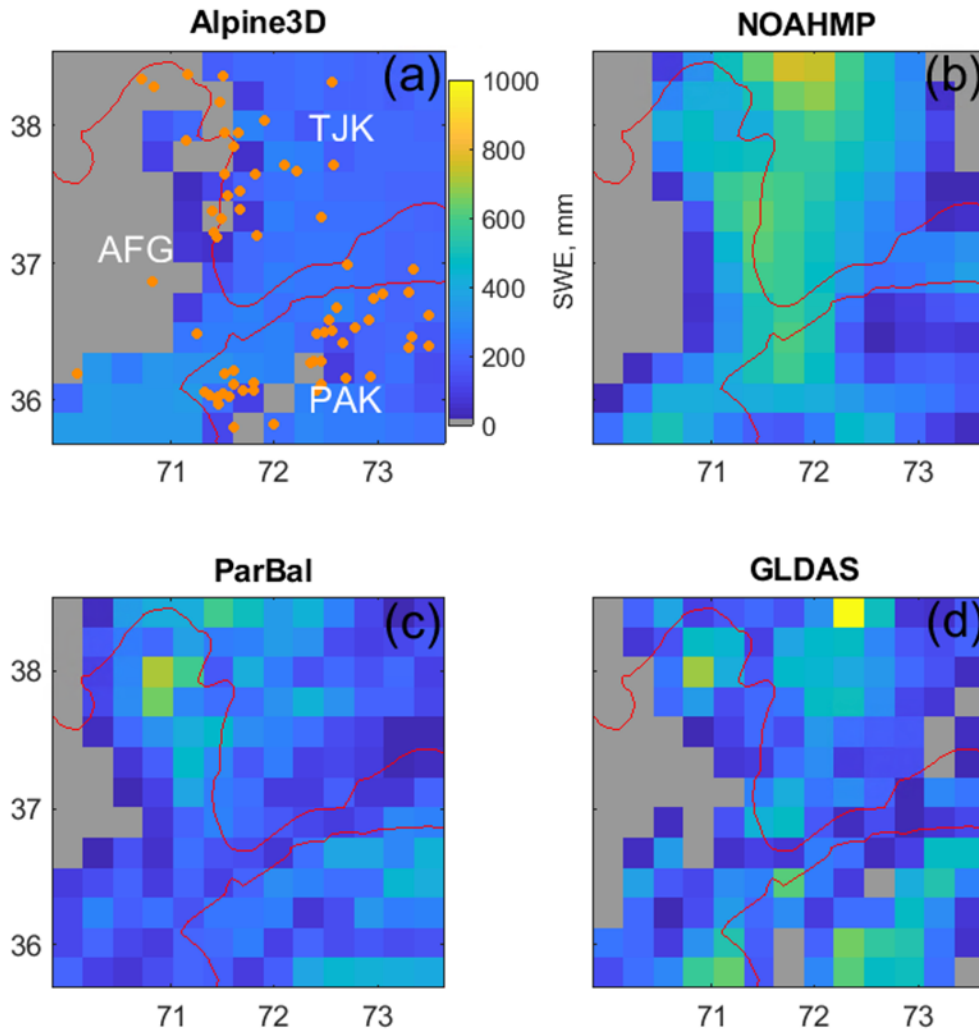


Figure 7 Four model (a-d) spatial comparison for the study area on 4 May 2018. The white letters are: AFG–Afghanistan; TJK–Tajikistan; and PAK–Pakistan. Also shown in (a) are the locations of the AKAH stations (orange points). This is a frame from a video sequence available as supplementary material.

385
 386 Since Alpine3D is relying heavily on extrapolation of SWE, we suggest its mean SWE values
 387 plotted in Figure 6 could have higher uncertainty than some of the other models. For example, the
 388 Alpine3D pixels seem to melt out early compared to the other models, especially ParBal, which is
 389 the only model relying on satellite-based estimates of fSCA (see supplementary video). Thus,
 390 Alpine3D may computing too little SWE in cold, high elevation areas that melt slowly. These
 391 problems are all indicative of stations that are located in valley bottoms and that only cover the
 392 lowest elevations across these 25 km pixels.

393

394 The ParBal results are confounding given that the agreement between the modeled SWE from
395 ParBal and SNOWPACK at individual AKAH stations (Figure 4ab) is much better for both 2017
396 and 2018.

397 For insight into potential biases in the modeled spatial SWE from ParBal, we carefully studied the
398 snow-covered area (SCA, not just for 2017 & 2018, but since 2001), the potential melt (i.e. the
399 melt if a pixel were 100% snow covered), and the melt from glacierized areas (light blue in Figure
400 1). We did not find any errors in the model, its parameters, or its forcings. Thus, it is possible that
401 the ParBal SWE is low-biased in 2017 for reasons that we could not discern, or that the other
402 models are high biased. Of note is that the 2017 & 2018 SCA (Figure 8 purple and orange)
403 is very similar for both years during the ablation period, especially at the end of the ablation season.

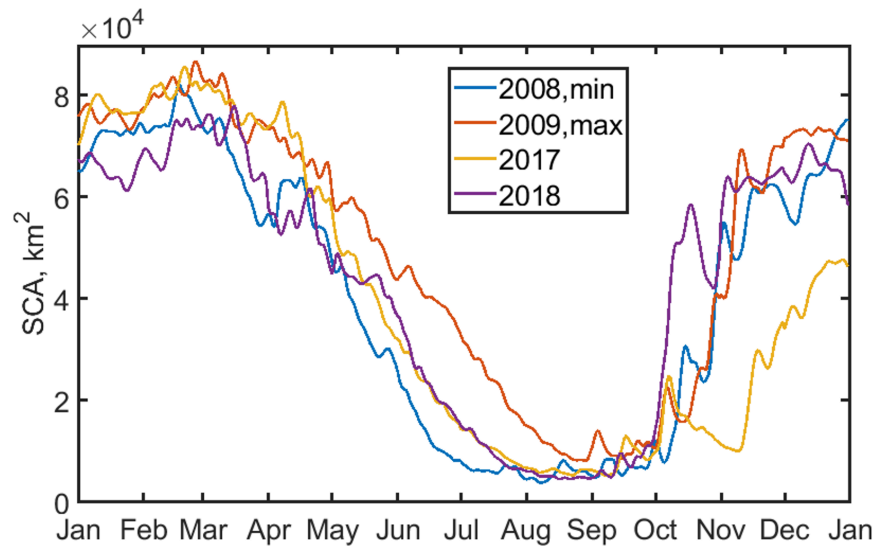


Figure 8 Time series of snow covered area from spatially and temporally interpolated MODSCAG (Rittger et al., in press), an input for ParBal, for four selected years across the region. Years 2008 and 2009 had the lowest and highest values on July 1 over the period of record from 2001 to 2018, while 2017 and 2018 comprise the AKAH station study period.

404 Since pixels do not contribute uniformly to melt, SCA alone cannot be used to predict SWE, but
405 in general years with less snow have lower SCA values towards the end of the ablation season.
406 Figure 8 shows that 2017 and 2018 were similar in terms of SCA from April through melt out.
407 Thus, the large difference between 2017 and 2018 for the AKAH station SWE, but small
408 differences in SCA and spatially-averaged reconstructed SWE, suggest that 2017 may have been
409 a larger snow year at the lower elevations where the AKAH stations are, but similar to 2018 at the
410 higher elevations.
411

412 6.3 Stratigraphy and stability

413 The simulated snow profiles from the AKAH stations (Figure 9ab) and the 25 km pixels containing
414 the AKAH stations (Figure 10ab) show very different snowpacks. Because of the induced increase
415 in elevation from scaling (e.g. from an average of 2619 m to 3858 m, Section 6.2), the 25 km pixels
416 show a deeper, but more faceted snowpack with critical layers that persist for a month or longer.
417 In 2017, for the median AKAH station values, the snowpack reaches a maximum of 76% facets

418 on January 21 (Figure 9a). In 2018, the snowpack reaches a maximum of 71% facets (Figure 9b).
 419 There were no critical layers simulated. In contrast, for the median values in the 25 km pixels for
 420 both years, the height of snow (HS) is approximately $2 \times$ that for the stations (Figure 10ab). The
 421 snowpack reaches a maximum of 94% facets in 2017, with one critical layer persisting for 35 days
 422 (Figure 10a). The snowpack in 2018 reaches 95% facets with 1 or 2 critical layers persisting for
 423 80 days (Figure 10b). During the Nuristan avalanches on 4 February to 7 February 2017 that killed
 424 over 100 people (United Nations, 2017), the AKAH stations show the largest 3-day snowfall of
 425 the study period (Figure 9a) and the results for the 25 km pixels show that large snowfall occurring
 426 on top of the only critical layer of the season (Figure 9b). That is a classic avalanche scenario, i.e.
 427 a large snowfall on a weak snowpack.

428 In lieu of any type of snow profile from this region, these profiles paint the best picture of the snow
 429 conditions available. A relatively stable snowpack seems to be present in the valleys, where the
 430 AKAH stations are located. But at the higher elevations, the simulated profiles show a more critical
 431 snowpack. This is especially serious considering these villages are in the runout zones of these
 432 potentially unstable snowpacks. In some cases, several thousand meters of vertical relief loom
 433 above the villages. For example, Yarkhun Lasht (36.795N 73.022E, el. 3249 m) in Pakistan is
 434 flanked by 6500 m peaks on both side of its valley.

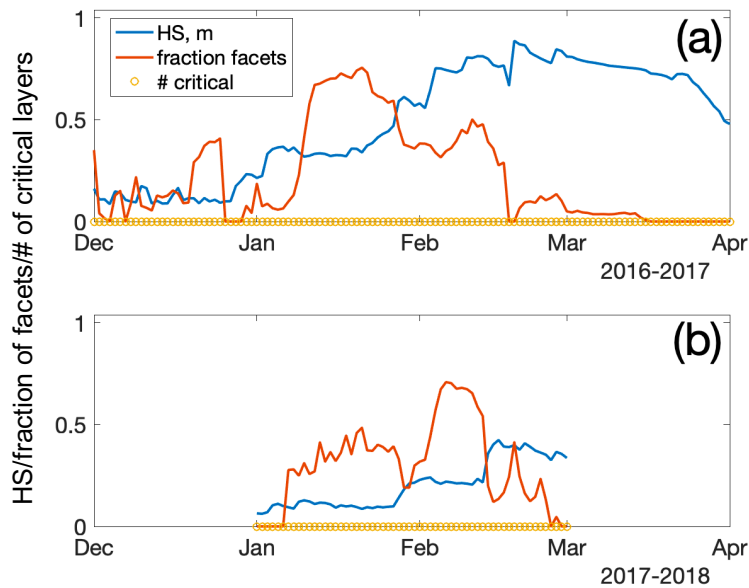


Figure 9 Stratigraphy summary of the AKAH stations for 2017 (a) and 2018 (b). Plotted are the median: height of snow (HS); fraction of the snowpack containing facets; and number of critical layers. The number of stations used to compute the medians varied due to snow coverage.

435

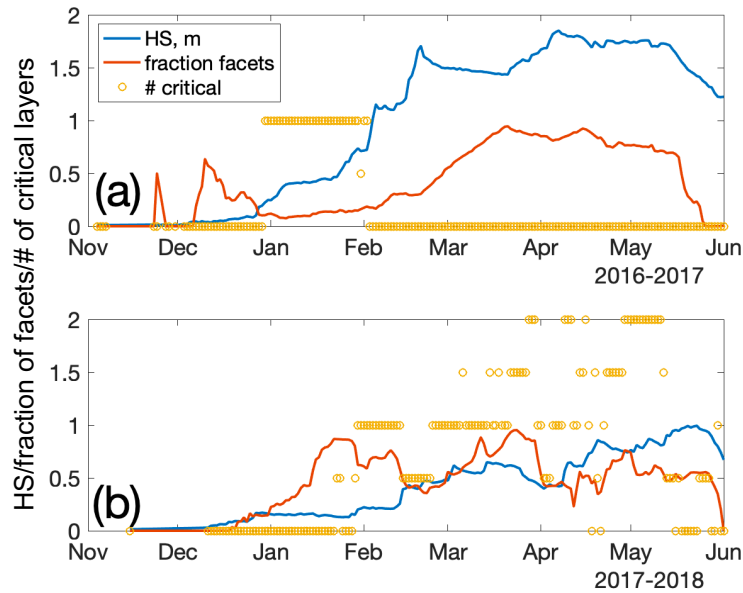


Figure 10 Stratigraphy summary of the (13x13) 25 km pixels containing AKAH stations for 2017 (a) and 2018 (b). Plotted are the median: height of snow (HS); fraction of the snowpack containing facets; and number of critical layers.

437

438 7 CONCLUSION

439 Knowledge of the snowpack in northwestern High Mountain Asia is poor. This area is subject to
 440 droughts and threatened by snow avalanches. Both problems can be aided by improved knowledge
 441 of the snowpack. Thanks to a novel operational avalanche observation network, there are now
 442 daily snow measurements at a number of operational weather stations in this austere region. In this
 443 study, two years of daily snow depth measurements from these stations were combined with
 444 downscaled reanalysis and remotely-sensed measurements to force a point and spatially distributed
 445 snow model. Compared to a previous effort (Bair et al., 2018a), this study represents a substantial
 446 improvement in SWE modeling for the region, and a first attempt to characterize region-wide snow
 447 stratigraphy. At the point scale, SWE estimates from a reconstruction technique that does not use
 448 precipitation or in situ measurements compared favorably. At the regional scale, four models
 449 showed a wide spread in both peak SWE and melt timing. For the models that rely on in situ
 450 precipitation measurements, a major challenge is spatial extrapolation, as many of the stations are
 451 located in deep valleys. Adding measurements from the mountains above would facilitate more
 452 realistic lapse rates, but these measurements do not currently exist, although they would be
 453 beneficial both for operational avalanche safety and for scientific studies.

454 In the regional comparison, SWE estimates from ParBal were on the low end, but given the model
 455 spread it is difficult to form a consensus estimate. We plan additional in situ validation at other
 456 sites in High Mountain Asia to continue to assess the performance of ParBal there.

457 The simulated profiles showed very different snowpacks. At the point scale at lower elevations in
 458 the valleys, profiles showed fewer facets and almost no critical layers, while at the regional scale

459 for higher elevations, the profiles showed heavily faceted snowpacks with critical layers that
460 persisted throughout the winter and spring.

461 8 CODE AND DATA AVAILABILITY

462 The code for ParBal is accessible at: <https://github.com/edwardbair/ParBal>

463 The code for MeteoIO, SNOWPACK, and Alpine3D are accessible at: <https://models.slf.ch/>

464 The code for NOAH-MP is accessible at: [https://ral.ucar.edu/solutions/products/noah-](https://ral.ucar.edu/solutions/products/noah-multiparameterization-land-surface-model-noah-mp-lsm)
465 [multiparameterization-land-surface-model-noah-mp-lsm](https://ral.ucar.edu/solutions/products/noah-multiparameterization-land-surface-model-noah-mp-lsm)

466 The GLDAS-2 and MERRA-2 forcings are accessible at: <https://disc.gsfc.nasa.gov/>

467 The reconstructed SWE and melt cubes are accessible at:
468 <ftp://ftp.snow.ucsb.edu/pub/org/snow/products/reconstruction/h23v05/500m/>

469 Unfortunately, the AKAH measurements are not publicly available due to security concerns.
470 Requests for the dataset should be made through The Aga Khan Agency for Habitat
471 (<https://www.akdn.org>).

472 **APPENDIX A Detailed model forcings and parameters**

473 *PARBAL*

474 ParBal was configured and forced as described in Bair et al. (2018a);Bair et al. (2016). The model
 475 time step was 1 hr. The DEM used was the ASTER GDEM version 2 at 1 arc sec (NASA JPL,
 476 2011), while the canopy type and fraction were taken from the Global Land Survey at 30 m (USGS,
 477 2009). The shortwave and longwave forcings were downscaled from the CERES SYN edition 4a
 478 1°/1 hr product (Rutan et al., 2015), while the air temperature, specific humidity, air pressure, and
 479 wind speeds were downscaled from the GLDAS NOAH version 2.1 0.25°/3 hr product (Cosgrove
 480 et al., 2003). Time-space smoothed (Dozier et al., 2008;Rittger et al., in press) fSCA and grain size
 481 from MODSCAG (Painter et al., 2009) was combined with the visible albedo degradation from
 482 dust in MODDRFS (Painter et al., 2012) to produce snow hourly snow albedo.

483 *NOAH-MP*

484 NOAH-MP v3.6 was run in retrospective mode within the NASA Land Information System (LIS)
 485 framework. A state vector ensemble (total 30 replicates) was generated by perturbing the forcings
 486 to account for the state uncertainty during forward propagation of the model. MERRA-2 (Gelaro
 487 et al., 2017) forcings were utilized with bilinear spatial and linear temporal interpolation. The
 488 model was run on an equidistant cylindrical grid with 0.25° spatial resolution and a 15 min model
 489 timestep. The spin-up time extended from May 2002 to May 2016 while the study period was from
 490 June 2016 to October 2018. The number of maximum layers in the snowpack was 3. Table A1
 491 provides details of the NOAH-MP scheme options selected. Further details regarding each scheme
 492 and relevant references can be found at: [https://ral.ucar.edu/solutions/products/noah-](https://ral.ucar.edu/solutions/products/noah-multiparameterization-land-surface-model-noah-mp-lsm)
 493 [multiparameterization-land-surface-model-noah-mp-lsm](https://ral.ucar.edu/solutions/products/noah-multiparameterization-land-surface-model-noah-mp-lsm).

| Physical process/ parameter | Scheme used |
|---|---|
| Elevation data | SRTM Native |
| Landcover data | MODIS Native (IGBPNCEP) |
| Slope, Albedo and Greenness data | NCEP Native |
| Bottom temperature (lapse-rate correction) | ISLSCP1 |
| Vegetation | dynamic |
| Canopy stomatal resistance | Ball-Berry |
| Runoff and groundwater | SIMGM |
| Surface layer drag coefficient | M-O (General Monin-Obukhov similarity theory) |
| Supercooled liquid water and frozen soil permeability | NY06 |
| Radiation transfer | gap=F(3D;cosz) |
| Snow surface albedo | BATS (Biosphere-Atmosphere Transfer Scheme) |

| | |
|------------------------------------|---------------|
| Rainfall and snowfall | Jordan91 |
| Snow and soil temperature time | semi-implicit |
| Lower boundary of soil temperature | Noah |

494 *Table A1 Noah-MP v3.6 physical parametrization scheme options utilized in this study.*

495 **SNOWPACK**

496 SNOWPACK v3.50 was run in research mode at a 15 min timestep with hourly outputs for each
497 of the AKAH stations. Hourly forcings were computed by combining temporally interpolated snow
498 depth from the AKAH manual measurements with: air temperature, incoming shortwave, reflected
499 shortwave, incoming longwave, wind speed, and relative humidity from the downscaled ParBal
500 outputs, as described in Section 5.2. SNOWPACK was only run for periods when measurements
501 from the AKAH stations were available, Nov/Dec to April/May, depending on the year.

502 Plots were assumed to be level, so forcings without terrain correction were applied except for
503 shading when the sun was below the local horizon, e.g. a mountain blocking the sun (Dozier and
504 Frew, 1990). The wind direction, which is not available in GLDAS-2, was fixed at the mean value
505 from the daily AKAH instantaneous values. The ground temperature was set as the minimum of
506 the air temperature or -1.5°C when snow cover was present.

507 Aside from setting required parameters and values for inputs and outputs, changes to default
508 parameters that affected model output are provided in Table A2:

| Parameters | Value | Description |
|-------------------------------|---------------|---|
| TS_DAYS_BETWEEN | 0.014666 days | Output hourly values |
| PRECIP_RATES | FALSE | Output is provided a summed precipitation over the output timestep (1 hr) |
| SW_MODE | BOTH | Both incoming and reflected (incoming x albedo) are provided |
| HEIGHT_OF_METEO_VALUES | 2 m | Height of meteorological measurements |
| HEIGHT_OF_WIND_VALUE | 2 m | Height of wind measurements |
| ENFORCE_MEASURED_SNOW_HEIGHTS | TRUE | Precipitation is calculated using HS |
| ATMOSPHERIC_STABILITY | NEUTRAL | Neutral conditions are often present in moderate to high wind speeds for mountain terrain (Lehning et al., 2002a; Mitterer and Schweizer, 2013) |
| MEAS_INCOMING_LONGWAVE | TRUE | Default is to estimate emissivity of the air and incoming longwave from |

| | | |
|--|--|--|
| | | other measured parameters (FALSE). Here we provide longwave forcings (TRUE). |
|--|--|--|

509 *Table A2 Model parameters for SNOWPACK*

510 *ALPINE3D*

511 Alpine3D version 3.10 was run using with the outputs produced by SNOWPACK as forcings for
512 each of the AKAH stations at 25 km resolution. The DEM and land cover (incorrectly labeled land
513 use in the Alpine3D documentation) data were upscaled from the ParBal data. Alpine3D was run
514 at an hourly timestep using hourly forcings, with daily outputs using the “enable-eb” switch. Other
515 switches were set to off, the defaults. The “enable-eb” switch computes the terrain radiation with
516 shading and terrain reflections (see Alpine 3D documentation at <https://models.slf.ch> for a
517 description).

518 To extend the length of the model runs, for each AKAH stations, GLDAS-2 precipitation was
519 appended to periods prior to the first AKAH observation for the year and after the last, as described
520 in Section 5.5.

521 The forcings were hourly: incoming shortwave, incoming longwave, air temperature, relative
522 humidity, wind speed, wind direction, reflected shortwave, accumulated precipitation, and ground
523 temperature.

524 Critical to Alpine3D are the interpolation methods from MeteIO to spatially distribute
525 precipitation and other forcings. We found the modeled SWE to be highly dependent on the spatial
526 interpolation of precipitation. Our initial approach was to explore local (i.e. with a given radius
527 from a station) and regional (i.e. all AKAH stations) lapse rates in the measured snow depth and
528 modeled precipitation from SNOWPACK. We found almost no correlation in many of the
529 measurements, not surprising given the complexity of the terrain and likely existence of
530 microclimates with substantial influence on precipitation. Without having a good validation source
531 for spatial precipitation (as is the case for all of High Mountain Asia), we selected an interpolation
532 method that yielded relatively smooth results, but showed increases in precipitation with elevation.

533 Ultimately, we decided to use an inverse distance weighting scheme with elevation detrending
534 (IDW_LAPSE) and a multilinear option. For this method, the input data are detrended, then the
535 residuals are spatially interpolated according to an inverse distance weighting scheme. The
536 detrending uses a multiple linear regression with northing, easting, and altitude. The linear
537 regression has an iterative method for removing outliers. Finally, values at each cell are retrended
538 using the multiple linear regression and added to the interpolated residuals.

539 A summary of the interpolation methods, all of which are defined in the MeteIO documentation
540 (Bavay and Egger, 2014), is given in Table A3.

| Forcing | Spatial interpolation method | Description and notes |
|-----------------|------------------------------|---|
| Air temperature | IDW_LAPSE | Inverse distance weighting with elevation detrending. |

| | | |
|-----------------------------|---|---|
| Accumulated precipitation | IDW_LAPSE with multilinear option set to TRUE | See notes above |
| Relative Humidity | LISTON_RH | See Liston and Elder (2006) |
| Precipitation phase | PPHASE | Simple splitting at 274.35K |
| Wind speed | IDW_LAPSE | See above |
| Incoming longwave radiation | AVG_LAPSE | Average filling with elevation lapse rate |
| Wind direction | CST | Constant, fixed at average value from AKAH station instantaneous measurements |
| Pressure | STD_PRESS | Standard atmospheric pressure with elevation |

541 *Table A3 Spatial interpolation methods for Alpine3D*

542 The same parameters as in Table A2 for SNOWPACK were used in Alpine3D with changes shown
543 in Table A4. Other parameters were defaults.

| Parameters | Value | Description |
|-------------------------------|--------|--|
| CALCULATION_STEP_LENGTH | 60 min | 1 hr model timestep |
| ENFORCE_MEASURED_SNOW_HEIGHTS | FALSE | Use accumulated precipitation estimate from SNOWPACK |

544 *Table A4 Model parameter changes for Alpine3D from Table A2*

545 AUTHOR CONTRIBUTION

546 DC provided the AKAH dataset. JA ran the NOAH MP simulations. KR prepared the snow surface
547 properties dataset. EB processed the data and prepared the manuscript.

548 COMPETING INTERESTS

549 The authors declare that they have no conflicts of interest.

550 ACKNOWLEDGMENTS

551 We are grateful to the Aga Khan Agency for Habitat for supplying the first snow measurements in
552 Afghanistan's watersheds since the 1980s. This work was supported by NASA Awards
553 80NSSC18K0427, 80NSSC18K1489, NASA 2015 HiMAT, and NNX17AC15G.

554
555 REFERENCES

556 Adam, J. C., Clark, E. A., Lettenmaier, D. P., and Wood, E. F.: Correction of global precipitation
557 products for orographic effects, *Journal of Climate*, 19, 15-38, 10.1175/JCLI3604.1, 2006.

558 Armstrong, R. L., Rittger, K., Brodzik, M. J., and others: Runoff from glacier ice and seasonal snow in
559 High Asia: separating melt water sources in river flow, *Regional Environmental Change*, 1-13,
560 <https://doi.org/10.1007/s10113-018-1429-0>, 2018.

561 Bair, E. H., Simenhois, R., Birkeland, K., and Dozier, J.: A field study on failure of storm snow slab
562 avalanches, *Cold Regions Science and Technology*, 79-80, 20-28, 10.1016/j.coldregions.2012.02.007,
563 2012.

564 Bair, E. H., Rittger, K., Davis, R. E., Painter, T. H., and Dozier, J.: Validating reconstruction of snow
565 water equivalent in California's Sierra Nevada using measurements from the NASA Airborne Snow
566 Observatory, *Water Resources Research*, 52, 8437-8460, 10.1002/2016WR018704, 2016.

567 Bair, E. H., Abreu Calfa, A., Rittger, K., and Dozier, J.: Using machine learning for real-time estimates of
568 snow water equivalent in the watersheds of Afghanistan, *The Cryosphere*, 12, 1579-1594, 10.5194/tc-12-
569 1579-2018, 2018a.

570 Bair, E. H., Davis, R. E., and Dozier, J.: Hourly mass and snow energy balance measurements from
571 Mammoth Mountain, CA USA, 2011–2017, *Earth Syst. Sci. Data*, 10, 549-563, 10.5194/essd-10-549-
572 2018, 2018b.

573 Bair, E. H., Rittger, K., Skiles, S. M., and Dozier, J.: An Examination of Snow Albedo Estimates From
574 MODIS and Their Impact on Snow Water Equivalent Reconstruction, *Water Resources Research*, 55,
575 7826-7842, 10.1029/2019wr024810, 2019.

576 Bartelt, P., and Lehning, M.: A physical SNOWPACK model for the Swiss avalanche warning: Part I:
577 numerical model, *Cold Regions Science and Technology*, 35, 123-145, 10.1016/s0165-232x(02)00074-5,
578 2002.

579 Bavay, M., and Egger, T.: MeteoIO 2.4.2: a preprocessing library for meteorological data, *Geosci. Model*
580 *Dev.*, 7, 3135-3151, 10.5194/gmd-7-3135-2014, 2014.

581 Bellaire, S., Jamieson, J. B., and Fierz, C.: Forcing the snow-cover model SNOWPACK with forecasted
582 weather data, *The Cryosphere*, 5, 1115-1125, 10.5194/tc-5-1115-2011, 2011.

583 Bellaire, S., van Herwijnen, A., Bavay, M., and Schweizer, J.: Distributed modeling of snow cover
584 instability at regional scale, *Proceedings of the 2018 International Snow Science Workshop*, Innsbruck,
585 Austria, 2018, 871-875,

586 Bookhagen, B., and Burbank, D. W.: Toward a complete Himalayan hydrological budget: Spatiotemporal
587 distribution of snowmelt and rainfall and their impact on river discharge, *Journal of Geophysical*
588 *Research: Earth Surface*, 115, 10.1029/2009jf001426, 2010.

589 Broxton, P. D., Zeng, X., and Dawson, N.: Why Do Global Reanalyses and Land Data Assimilation
590 Products Underestimate Snow Water Equivalent?, *J. Hydrometeorol.*, 17, 2743-2761, 10.1175/jhm-d-16-
591 0056.1, 2016.

592 Burt, P., and Adelson, E.: The Laplacian pyramid as a compact image code, *IEEE Transactions on*
593 *Communications*, 31, 532-540, 10.1109/TCOM.1983.1095851, 1983.

594 Chabot, D., and Kaba, A.: Avalanche forecasting in the central Asian countries of Afghanistan, Pakistan
595 and Tajikistan, *Proc. 2016 Intl. Snow Sci. Wksp.*, Breckenridge, CO, 2016.

596 Chen, F., Barlage, M., Tewari, M., Rasmussen, R., Jin, J., Lettenmaier, D., Livneh, B., Lin, C., Miguez-
597 Macho, G., Niu, G.-Y., Wen, L., and Yang, Z.-L.: Modeling seasonal snowpack evolution in the complex
598 terrain and forested Colorado Headwaters region: A model intercomparison study, *Journal of Geophysical*
599 *Research: Atmospheres*, 119, 13,795-713,819, 10.1002/2014jd022167, 2014.

600 Cornwell, E., Molotch, N. P., and McPhee, J.: Spatio-temporal variability of snow water equivalent in the
601 extra-tropical Andes Cordillera from distributed energy balance modeling and remotely sensed snow
602 cover, *Hydrol. Earth Syst. Sci.*, 20, 411-430, 10.5194/hess-20-411-2016, 2016.

603 Cosgrove, B. A., Lohmann, D., Mitchell, K. E., Houser, P. R., Wood, E. F., Schaake, J. C., Robock, A.,
604 Marshall, C., Sheffield, J., Duan, Q., Luo, L., Higgins, R. W., Pinker, R. T., Tarpley, J. D., and Meng, J.:
605 Real-time and retrospective forcing in the North American Land Data Assimilation System (NLDAS)
606 project, *Journal of Geophysical Research: Atmospheres*, 108, 8842, 10.1029/2002JD003118, 2003.

607 Dahri, Z. H., Ludwig, F., Moors, E., Ahmad, B., Khan, A., and Kabat, P.: An appraisal of precipitation
608 distribution in the high-altitude catchments of the Indus basin, *Science of The Total Environment*, 548-
609 549, 289-306, <https://doi.org/10.1016/j.scitotenv.2016.01.001>, 2016.

610 Dahri, Z. H., Moors, E., Ludwig, F., Ahmad, S., Khan, A., Ali, I., and Kabat, P.: Adjustment of
611 measurement errors to reconcile precipitation distribution in the high-altitude Indus basin, *Int. J.*
612 *Climatol.*, 38, 3842-3860, 10.1002/joc.5539, 2018.

613 Dozier, J., and Frew, J.: Rapid calculation of terrain parameters for radiation modeling from digital
614 elevation data, *IEEE Transactions on Geoscience and Remote Sensing*, 28, 963-969, 10.1109/36.58986,
615 1990.

616 Dozier, J., Painter, T. H., Rittger, K., and Frew, J. E.: Time-space continuity of daily maps of fractional
617 snow cover and albedo from MODIS, *Advances in Water Resources*, 31, 1515-1526,
618 10.1016/j.advwatres.2008.08.011, 2008.

619 Ek, M. B., Mitchell, K. E., Lin, Y., Rogers, E., Grunmann, P., Koren, V., Gayno, G., and Tarpley, J. D.:
620 Implementation of Noah land surface model advances in the National Centers for Environmental
621 Prediction operational mesoscale Eta model, *Journal of Geophysical Research: Atmospheres*, 108,
622 10.1029/2002jd003296, 2003.

623 Fierz, C., Armstrong, R. L., Durand, Y., Etchevers, P., Greene, E., McClung, D. M., Nishimura, K.,
624 Satyawali, P. K., and Sokratov, S.: The International Classification for Seasonal Snow on the Ground,
625 IHP-VII Technical Documents in Hydrology N°83, 90, 2009.

626 Gelaro, R., McCarty, W., Suárez, M. J., Todling, R., Molod, A., Takacs, L., Randles, C. A., Darmenov,
627 A., Bosilovich, M. G., Reichle, R., Wargan, K., Coy, L., Cullather, R., Draper, C., Akella, S., Buchard,
628 V., Conaty, A., Silva, A. M. d., Gu, W., Kim, G.-K., Koster, R., Lucchesi, R., Merkova, D., Nielsen, J. E.,
629 Partyka, G., Pawson, S., Putman, W., Rienecker, M., Schubert, S. D., Sienkiewicz, M., and Zhao, B.: The
630 Modern-Era Retrospective Analysis for Research and Applications, Version 2 (MERRA-2), *Journal of*
631 *Climate*, 30, 5419-5454, 10.1175/jcli-d-16-0758.1, 2017.

632 Goodison, B., Louie, P. Y. T., and Yang, D.: WMO Solid precipitation measurement intercomparison,
633 World Meteorological Organization, 1998.

634 Harris, I., Jones, P. D., Osborn, T. J., and Lister, D. H.: Updated high-resolution grids of monthly climatic
635 observations – the CRU TS3.10 Dataset, *Int. J. Climatol.*, 34, 623-642, 10.1002/joc.3711, 2014.

- 636 Hirashima, H., Yamaguchi, S., Sato, A., and Lehning, M.: Numerical modeling of liquid water movement
637 through layered snow based on new measurements of the water retention curve, *Cold Regions Science*
638 and *Technology*, 64, 94-103, <https://doi.org/10.1016/j.coldregions.2010.09.003>, 2010.
- 639 Huffman, G. J., Bolvin, D. T., Nelkin, E. J., Wolff, D. B., Adler, R. F., Gu, G., Hong, Y., Bowman, K. P.,
640 and Stocker, E. F.: The TRMM Multisatellite Precipitation Analysis (TMPA): Quasi-Global, Multiyear,
641 Combined-Sensor Precipitation Estimates at Fine Scales, *J. Hydrometeorol.*, 8, 38-55, 10.1175/jhm560.1,
642 2007.
- 643 Immerzeel, W. W., Wanders, N., Lutz, A. F., Shea, J. M., and Bierkens, M. F. P.: Reconciling high-
644 altitude precipitation in the upper Indus basin with glacier mass balances and runoff, *Hydrol. Earth Syst.*
645 *Sci.*, 19, 4673-4687, 10.5194/hess-19-4673-2015, 2015.
- 646 Jamieson, J. B.: The compression test – after 25 years, *The Avalanche Review*, 18, 10-12, 1999.
- 647 Jepsen, S. M., Molotch, N. P., Williams, M. W., Rittger, K. E., and Sickman, J. O.: Interannual variability
648 of snowmelt in the Sierra Nevada and Rocky Mountains, United States: Examples from two alpine
649 watersheds, *Water Resources Research*, 48, W02529, 10.1029/2011WR011006, 2012.
- 650 Kochendorfer, J., Rasmussen, R., Wolff, M., Baker, B., Hall, M. E., Meyers, T., Landolt, S., Jachcik, A.,
651 Isaksen, K., Brækkan, R., and Leeper, R.: The quantification and correction of wind-induced precipitation
652 measurement errors, *Hydrol. Earth Syst. Sci.*, 21, 1973-1989, 10.5194/hess-21-1973-2017, 2017.
- 653 Lehning, M., Bartelt, P., Brown, B., and et. al: SNOWPACK model calculations for avalanche warning
654 based upon a new network of weather and snow stations, *Cold Reg. Sci. Technol.*, 30, 145-157, 1999.
- 655 Lehning, M., Bartelt, P., Brown, B., and Fierz, C.: A physical SNOWPACK model for the Swiss
656 avalanche warning: Part III: meteorological forcing, thin layer formation and evaluation, *Cold Regions*
657 *Science and Technology*, 35, 169-184, 10.1016/S0165-232X(02)00072-1, 2002a.
- 658 Lehning, M., Bartelt, P., Brown, B., Fierz, C., and Satyawali, P.: A physical SNOWPACK model for the
659 Swiss avalanche warning, Part II: Snow microstructure, *Cold Regions Science and Technology*, 35, 147-
660 167, doi: 10.1016/S0165-1232X(1002)00073-00073, 2002b.
- 661 Lehning, M., Völksch, I., Gustafsson, D., Nguyen, T. A., Stähli, M., and Zappa, M.: ALPINE3D: a
662 detailed model of mountain surface processes and its application to snow hydrology, *Hydrological*
663 *Processes*, 20, 2111-2128, 10.1002/hyp.6204, 2006.
- 664 Liston, G. E., and Elder, K.: A meteorological distribution system for high-resolution terrestrial modeling
665 (MicroMet), *J. Hydrometeorol.*, 7, 217–234, 10.1175/JHM486.1, 2006.
- 666 Lutz, A. F., Immerzeel, W. W., Shrestha, A. B., and Bierkens, M. F. P.: Consistent increase in High
667 Asia’s runoff due to increasing glacier melt and precipitation, *Nature Climate Change*, 4, 587,
668 10.1038/nclimate2237, 2014.
- 669 Margulis, S. A., Cortés, G., Giroto, M., and Durand, M.: A Landsat-Era Sierra Nevada Snow Reanalysis
670 (1985–2015), *J. Hydrometeorol.*, 17, 1203-1221, 10.1175/jhm-d-15-0177.1, 2016.
- 671 Marks, D., and Dozier, J.: Climate and energy exchange at the snow surface in the alpine region of the
672 Sierra Nevada, 2, *Snow cover energy balance*, *Water Resources Research*, 28, 3043-3054,
673 10.1029/92WR01483, 1992.

- 674 Martinec, J., and Rango, A.: Areal distribution of snow water equivalent evaluated by snow cover
675 monitoring, *Water Resources Research*, 17, 1480-1488, 10.1029/WR017i005p01480, 1981.
- 676 Milly, P. C. D., and Dunne, K. A.: Macroscale water fluxes 1. Quantifying errors in the estimation of
677 basin mean precipitation, *Water Resources Research*, 38, 23-21-23-14, 10.1029/2001WR000759, 2002.
- 678 Mitterer, C., and Schweizer, J.: Analysis of the snow-atmosphere energy balance during wet-snow
679 instabilities and implications for avalanche prediction, *The Cryosphere*, 7, 205-216, 10.5194/tc-7-205-
680 2013, 2013.
- 681 Molotch, N. P.: Reconstructing snow water equivalent in the Rio Grande headwaters using remotely
682 sensed snow cover data and a spatially distributed snowmelt model, *Hydrological Processes*, 23, 1076-
683 1089, 10.1002/hyp.7206, 2009.
- 684 Monti, F., Schweizer, J., and Fierz, C.: Hardness estimation and weak layer detection in simulated snow
685 stratigraphy, *Cold Regions Science and Technology*, 103, 82-90,
686 <https://doi.org/10.1016/j.coldregions.2014.03.009>, 2014.
- 687 Nishimura, K., Baba, E., Hirashima, H., and Lehning, M.: Application of the snow cover model
688 SNOWPACK to snow avalanche warning in Niseko, Japan, *Cold Regions Science and Technology*, 43,
689 62-70, <https://doi.org/10.1016/j.coldregions.2005.05.007>, 2005.
- 690 Niu, G.-Y., and Yang, Z.-L.: Effects of vegetation canopy processes on snow surface energy and mass
691 balances, *Journal of Geophysical Research: Atmospheres*, 109, 10.1029/2004jd004884, 2004.
- 692 Niu, G.-Y., Yang, Z.-L., Mitchell, K. E., Chen, F., Ek, M. B., Barlage, M., Kumar, A., Manning, K.,
693 Niyogi, D., Rosero, E., Tewari, M., and Xia, Y.: The community Noah land surface model with
694 multiparameterization options (Noah-MP): 1. Model description and evaluation with local-scale
695 measurements, *Journal of Geophysical Research: Atmospheres*, 116, 10.1029/2010jd015139, 2011.
- 696 Painter, T. H., Rittger, K., McKenzie, C., Slaughter, P., Davis, R. E., and Dozier, J.: Retrieval of subpixel
697 snow-covered area, grain size, and albedo from MODIS, *Remote Sensing of Environment*, 113, 868-879,
698 10.1016/j.rse.2009.01.001, 2009.
- 699 Painter, T. H., Bryant, A. C., and Skiles, S. M.: Radiative forcing by light absorbing impurities in snow
700 from MODIS surface reflectance data, *Geophysical Research Letters*, 39, L17502,
701 10.1029/2012GL052457, 2012.
- 702 Painter, T. H., Berisford, D. F., Boardman, J. W., Bormann, K. J., Deems, J. S., Gehrke, F., Hedrick, A.,
703 Joyce, M., Laidlaw, R., Marks, D., Mattmann, C., McGurk, B., Ramirez, P., Richardson, M., Skiles, S.
704 M., Seidel, F. C., and Winstal, A.: The Airborne Snow Observatory: Fusion of scanning lidar, imaging
705 spectrometer, and physically-based modeling for mapping snow water equivalent and snow albedo,
706 *Remote Sensing of Environment*, 184, 139-152, 10.1016/j.rse.2016.06.018, 2016.
- 707 Raup, B., Racoviteanu, A., Khalsa, S. J. S., Helm, C., Armstrong, R., and Arnaud, Y.: The GLIMS
708 geospatial glacier database: A new tool for studying glacier change, *Global and Planetary Change*, 56,
709 101-110, <https://doi.org/10.1016/j.gloplacha.2006.07.018>, 2007.
- 710 Rienecker, M. M., Suarez, M. J., Gelaro, R., Todling, R., Julio Bacmeister, Liu, E., Bosilovich, M. G.,
711 Schubert, S. D., Takacs, L., Kim, G.-K., Bloom, S., Chen, J., Collins, D., Conaty, A., Silva, A. d., Gu, W.,
712 Joiner, J., Koster, R. D., Lucchesi, R., Molod, A., Owens, T., Pawson, S., Pegion, P., Redder, C. R.,

713 Reichle, R., Robertson, F. R., Ruddick, A. G., Sienkiewicz, M., and Woollen, J.: MERRA: NASA's
714 Modern-Era Retrospective Analysis for Research and Applications, *Journal of Climate*, 24, 3624-3648,
715 10.1175/jcli-d-11-00015.1, 2011.

716 Rittger, K., Bair, E. H., Kahl, A., and Dozier, J.: Spatial estimates of snow water equivalent from
717 reconstruction, *Advances in Water Resources*, 94, 345-363, 10.1016/j.advwatres.2016.05.015, 2016.

718 Rittger, K., Raleigh, M. S., Dozier, J., Hill, A. F., Lutz, J. A., and Painter, T. H.: Canopy Adjustment and
719 Improved Cloud Detection for Remotely Sensed Snow Cover Mapping, *Water Resources Research*, in
720 press.

721 Rodell, M., Houser, P. R., Jambor, U., Gottschalck, J., Mitchell, K., Meng, C. J., Arsenault, K., Cosgrove,
722 B., Radakovich, J., Bosilovich, M., Entin, J. K., Walker, J. P., Lohmann, D., and Toll, D.: The Global
723 Land Data Assimilation System, *Bulletin of the American Meteorological Society*, 85, 381-394,
724 10.1175/BAMS-85-3-381, 2004.

725 Rutan, D. A., Kato, S., Doelling, D. R., Rose, F. G., Nguyen, L. T., Caldwell, T. E., and Loeb, N. G.:
726 CERES synoptic product: Methodology and validation of surface radiant flux, *J. Atmos. Ocean. Technol.*,
727 32, 1121-1143, 10.1175/JTECH-D-14-00165.1, 2015.

728 Schweizer, J., and Jamieson, B.: Snow cover properties for skier triggering of avalanches, *Cold Regions
729 Science and Technology*, 33, 207-221, 10.1016/s0165-232x(01)00039-8, 2001.

730 Schweizer, J., and Jamieson, B.: A threshold sum approach to stability evaluation of manual snow
731 profiles, *Cold Regions Science and Technology*, 47, 50-59, 10.1016/j.coldregions.2006.08.011, 2007.

732 Shakoor, A., and Ejaz, N.: Flow Analysis at the Snow Covered High Altitude Catchment via Distributed
733 Energy Balance Modeling, *Scientific Reports*, 9, 4783, 10.1038/s41598-019-39446-1, 2019.

734 Skiles, S. M., and Painter, T.: Daily evolution in dust and black carbon content, snow grain size, and
735 snow albedo during snowmelt, Rocky Mountains, Colorado, *Journal of Glaciology*, 63, 118-132,
736 10.1017/jog.2016.125, 2016.

737 Smith, T., and Bookhagen, B.: Changes in seasonal snow water equivalent distribution in High Mountain
738 Asia (1987 to 2009), *Science Advances*, 4, e1701550, 10.1126/sciadv.1701550, 2018.

739 Sturm, M., Holmgren, J., and Liston, G. E.: A seasonal snow cover classification system for local to
740 global applications, *Journal of Climate*, 8, 1261-1283, 10.1175/1520-
741 0442(1995)008<1261:ASSCCS>2.0.CO;2, 1995.

742 Sturm, M., Taras, B., Liston, G. E., Derksen, C., Jonas, T., and Lea, J.: Estimating snow water equivalent
743 using snow depth data and climate classes, *J. Hydrometeorol.*, 11, 1380-1394, 10.1175/2010jhm1202.1,
744 2010.

745 Tan, B., Woodcock, C. E., Hu, J., Zhang, P., Ozdogan, M., Huang, D., Yang, W., Knyazikhin, Y., and
746 Myneni, R. B.: The impact of gridding artifacts on the local spatial properties of MODIS data:
747 Implications for validation, compositing, and band-to-band registration across resolutions, *Remote
748 Sensing of Environment*, 105, 98-114, 10.1016/j.rse.2006.06.008, 2006.

749 United Nations: Afghanistan: Nuristan avalanche, update to flash report (as of 8 February 2017), Office
750 for the Coordination of Humanitarian Affairs (OCHA), 2017.

- 751 USAID: Afghanistan Food Security Update, FEWS Net, Washington, DC, 4, 2008.
- 752 Global Land Survey: <http://glcfapp.glcf.umd.edu/data/gls/>, access: 1 September 2017, 2009.
- 753 van Herwijnen, A., and Jamieson, B.: Fracture character in compression tests, *Cold Regions Science and*
754 *Technology*, 47, 60-68, 10.1016/j.coldregions.2006.08.016, 2007.
- 755 Viste, E., and Sorteberg, A.: Snowfall in the Himalayas: an uncertain future from a little-known past, *The*
756 *Cryosphere*, 9, 1147-1167, 10.5194/tc-9-1147-2015, 2015.
- 757 Xia, Y., Mitchell, K., Ek, M., Sheffield, J., Cosgrove, B., Wood, E., Luo, L., Alonge, C., Wei, H., Meng,
758 J., Livneh, B., Lettenmaier, D., Koren, V., Duan, Q., Mo, K., Fan, Y., and Mocko, D.: Continental-scale
759 water and energy flux analysis and validation for the North American Land Data Assimilation System
760 project phase 2 (NLDAS-2): 1. Intercomparison and application of model products, *Journal of*
761 *Geophysical Research: Atmospheres*, 117, D03109, 10.1029/2011JD016048, 2012.
- 762 Xiaoxiong, X., Nianzeng, C., and Barnes, W.: Terra MODIS on-orbit spatial characterization and
763 performance, *IEEE Transactions on Geoscience and Remote Sensing*, 43, 355-365,
764 10.1109/TGRS.2004.840643, 2005.
- 765 Yang, Z.-L., and Niu, G.-Y.: The Versatile Integrator of Surface and Atmosphere processes: Part 1.
766 Model description, *Global and Planetary Change*, 38, 175-189, [https://doi.org/10.1016/S0921-](https://doi.org/10.1016/S0921-8181(03)00028-6)
767 [8181\(03\)00028-6](https://doi.org/10.1016/S0921-8181(03)00028-6), 2003.
- 768 Yatagai, A., Kamiguchi, K., Arakawa, O., Hamada, A., Yasutomi, N., and Kitoh, A.: APHRODITE:
769 Constructing a Long-Term Daily Gridded Precipitation Dataset for Asia Based on a Dense Network of
770 Rain Gauges, *Bulletin of the American Meteorological Society*, 93, 1401-1415, 10.1175/bams-d-11-
771 00122.1, 2012.
- 772